Збірник праць Інституту математики НАН України 2015, т. 12, № 5, 275–283

УДК 532.595

Natural sloshing frequencies and modes in an upright circular container with poles*

A. N. Timokha

Institute of Mathematics of NAS of Ukraine, Kiev, Ukraine;
Centre of Excellence AMOS, Norwegian University of Science and Technology, Trondheim, Norway

Natural sloshing modes are approximated, semi-analytically, for an upright circular cylindrical tank equipped with an array of vertical poles (pipes) as it happens, e.g., in shafts of ocean platforms.

Отримано чисельно–аналітичні наближення власних форм коливання рідини у вертикальному циліндричному контейнері, в якому встановлено вертикальні стовпи (труби), як то буває, наприклад, в шахтах океанських платформ.

1. Introduction

Interior space of tanks contains, normally, devices and structures [2, ch. 1] which play different roles, that includes, suppression of sloshing and stiffening the construction. Vertical pipes (poles) are installed, e.g., in shafts of ocean platforms [1]/cooling tanks of nuclear reactors [7]. The poles modify the natural sloshing modes and frequencies as well as cause an extra damping due to flow separation [2, ch. 6]. The both effects are poorly investigated. This inhibits progress of analytical approaches to nonlinear sloshing problems for those tanks.

The present paper constructs an analytically approximate solution of the spectral boundary problem on the natural sloshing modes for an

* The work was partly supported by the Grant № 0112U001015. The author also acknowledges the financial support of the Centre of Autonomous Marine Operations and Systems (AMOS) whose main sponsor is the Norwegian Research Council (Project number 223254–AMOS).

upright circular cylindrical tank with an array of vertical poles. The Trefftz variational method is adopted that facilitates efficient computations and parameter studies *versus* position, number and radii of the poles. Numerical examples are mainly associated with computations in [1].

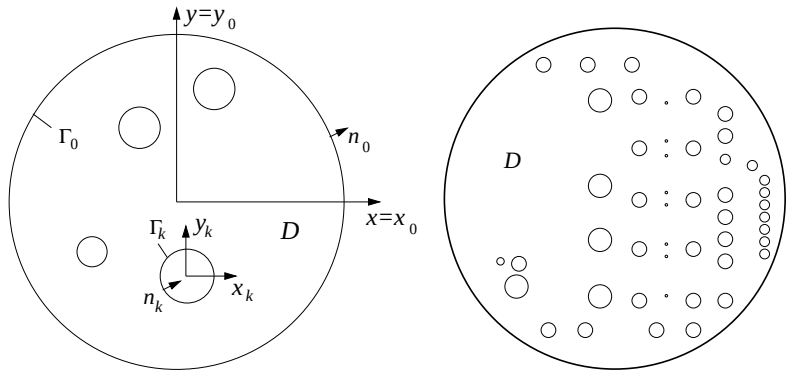

Fig. 1. *The left panel*: Geometric notations to the spectral boundary problem (1) in a circular cheese–like domain D associated with the cross–sectional area of an upright circular cylindrical tank equipped with vertical poles. The domain is confined by the external (circular) boundary Γ_0 and has, in addition, circular holes Γ_k, $k = 1, \ldots, M$. The outer normal $\boldsymbol{n}$ to D is the same as the set of $\boldsymbol{n}_k$ on Γ_k, $k = 0, \ldots, M$. The solution method requires introducing the local Cartesian $O_k x_k y_k$ ($O_0 x_0 y_0 = Oxy$) and polar (r_k, θ_k), $k = 0, \ldots, M$ coordinates. *The right panel:* A schematic cross-sectional plan of the Draugen platform at the sea level (dimensions are reported in [1]).

2. Statement of the problem

The spectral (eigenvalue) boundary problem on natural sloshing modes and frequencies in an upright cylindrical tank admits separation of the vertical coordinate z and, thereby, reduces to the boundary eigenvalue problem in the cross–sectional area D (see, an extensive discussion, e.g., in [2, ch. 4] and [1]). When choosing the Oxy plane coinciding with the flat mean free surface and h is the mean liquid depth, separating z implies the natural sloshing modes $\Phi(x, y, z; \lambda) = \varphi(x, y; \lambda) \cosh(\lambda(z + h))/\cosh(\lambda h)$ where $\varphi(x, y; \lambda)$ ($\lambda > 0$, the trivial solution $\lambda = 0, \Phi = \varphi = \text{const}$ does not satisfies the volume conservation condition and should

be excluded) comes from the well–known spectral boundary problem

$$-\nabla^2\varphi = \lambda\varphi \ \text{ in } \ D; \ \ \partial_n\varphi = 0 \ \text{ on } \ \partial D; \ \ \lambda > 0 \tag{1}$$

for the Laplace operator $\Delta = \nabla^2$. The natural sloshing frequencies are then computed by $\sigma = \sqrt{g\lambda \tanh(\lambda h)}$ where g is the gravity acceleration.

Domain D and its boundary $\partial D = \cup_{k=0}^{M}\Gamma_k$ are shown in fig. 1 (the left panel introduces, schematically, geometric notations, but the right panel illustrates the actual geometry for the Draugen platform shaft). Circles Γ_k have the radii R_k and their centres are at (x_{0k}, y_{0k}) in the global Cartesian coordinates Oxy. Henceforth, (1) is scaled by R_0 that suggests $h := h/R_0$, $R_0 = 1$, $R_k := R_k/R_0, x_{0k} := x_{0k}/R_0, y_{0k} := y_{0k}/R_0$, $k = 0, \ldots, M$ and so on.

Remark 2.5. The spectral problem (1) has exact analytical solutions for $M = 0$ (no holes, a purely circular cylindrical tank) and $M = 1$ when the origins coincide, $O_0 = O_1$ (an annular cylindrical tank). These solutions are documented, in some detail, in [2, 4, 6]. Eigenvalues λ are then computed from a *transcendental equation* involving the Bessel functions. This is even though (1) is a linear spectral problem which reduces, naturally, to a *linear algebraic problem* when using traditional numerical methods. The latter methods do not provide the analytical solutions and, generally speaking, demonstrate a rather low convergence [1, 5, 7] to the exact analytical λ.

Remark 2.6. A rough approximation of the natural sloshing frequencies (and, therefore, λ) can also be found utilising the strip theory and the Reynolds quotient formulation of the original spectral sloshing problem ([1] and [2, ch. 4]). This is, generally, unable to construct the natural sloshing modes (required in the analytical sloshing), assumes, explicitly, that the poles are located far from each other (the proximity effect is neglected) and their radii R_i, $i \geq 1$ are small relative to R_0.

3. Solution method

The present paper uses a variational Trefftz method which suggests a λ-depending representation of $\varphi(x, y; \lambda)$ and trial functions $\delta\varphi(x, y; \lambda)$ so that getting $\lambda > 0$ and $\varphi(x, y; \lambda)$ follows from the variational equation [3]

$$\int_{\partial D} \partial_n\varphi \, \delta\varphi \, d\Gamma \equiv \sum_{k=0}^{M} \int_{\Gamma_k} (\nabla\varphi \cdot \boldsymbol{n_k}) \, \delta\varphi \, d\Gamma = 0. \tag{2}$$

The eigenfunction φ is furthermore posed as

$$\varphi(x,y;\lambda)=\sum_{k=0}^{M}\sum_{i=0}^{2N_k} a_{k,i}\,\phi_{k,i}(r_k,\theta_k;\lambda),\quad N_k\to\infty, \tag{3}$$

where λ and $\{a_{k,i}\}$ are the unknowns, but the functional basis $\{\phi_{k,i}\}$ consists of

$$\begin{aligned}\{\phi_{0,i}(x,y;\lambda),\ i=0,\dots,2N_0\}=\{&J_0(\lambda r_0),J_1(\lambda r_0)\cos\theta_0,\dots,\\ &J_{N_0}(\lambda r_0)\cos N_0\theta_0,J_1(\lambda r_0)\sin\theta_0,\dots,J_{N_0}(\lambda r_0)\sin N_0\theta_0\},\end{aligned} \tag{4}$$

$$\begin{aligned}\{\phi_{k,i}(x,y;\lambda),\ i=0,\dots,2N_k\}=\{&Y_0(\lambda r_k),Y_1(\lambda r_k)\cos\theta_k,\dots,\\ &Y_{N_k}(\lambda r_k)\cos N_k\theta_k,\\ &Y_1(\lambda r_k)\sin\theta_k,\dots,Y_{N_k}(\lambda r_k)\sin N_k\theta_k\},\ k=1,\dots,M,\end{aligned} \tag{5}$$

defined in the polar coordinates (r_k,θ_k) but considered, altogether, as functions of x,y and λ; $J_l(\cdot)$ and $Y_l(\cdot)$ are the Bessel functions of the first and second kinds, respectively, and $\lambda>0$. The functional subset (4) approximates a "regular" component (no singularities inside the circles Γ_k, $k=1,\dots,M$), but (5) fits the local singular behaviour of $\varphi(x,y;\lambda)$ inside the circular holes. The functional set (4), (5) is complete since the Dirichlet and Neumann traces of $\{\phi_{l,i}\}$ on $\Gamma_l=\{x=x_{l0}+R_l\cos\theta_l,\ y=x_{l0}+R_l\sin\theta_l;\ 0\le\theta_l<2\pi\}$ are, within to multipliers, the 2π–periodic Fourier basis.

Substituting (3) into (2) within $\delta\varphi=\phi_{n,j}$ gives the $\left[\sum_{k=0}^{M}(2N_k+1)\right]\times\left[\sum_{k=0}^{M}(2N_k+1)\right]$ system of linear *homogeneous* algebraic equations

$$\sum_{k=0}^{M}\sum_{i=0}^{2N_k}\underbrace{\left[\sum_{l=0}^{M}R_l\int_0^{2\pi}\left[(\nabla\phi_{k,i}|_{\Gamma_l}\cdot\boldsymbol{n}_l)\,\phi_{n,j}\right]_{\Gamma_l}d\theta_l\right]}_{B_{(n,j)(k,i)}(\lambda)}a_{k,i}=0 \tag{6}$$

with respect to $\{a_{k,i}\}$ and the symmetric matrix ($B_{(n,j)(k,i)}=B_{(k,i)(n,j)}$ due to the second Green identity) must have the zero-determinant

$$\det\{B_{(n,j)(k,i)}(\lambda)\}=0 \tag{7}$$

which is, in fact, a transcendental equation with respect to λ in terms of the Bessel functions.

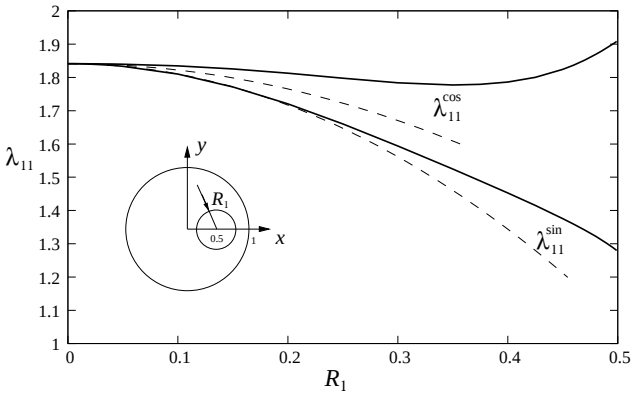

Fig. 2. Two lowest eigenvalues $\lambda_{11}^{\sin}$ and $\lambda_{11}^{\cos}$ splitting from $\lambda_{11} = 1.841\ldots$; $J_1'(\lambda_{11}) = 0$ for D without holes (the corresponding exact analytical eigenfunctions are then $J_1(\lambda r)\sin\theta$ and $J_1(\lambda r)\cos\theta$) when a single eccentric pole of the nondimensional radius $0 < R_1 < 0.5$ is installed with the $x = 0.5$-offset. The computed values of $\lambda_{11}^{\sin}$ and $\lambda_{11}^{\cos}$ *versus* R_1 are marked by the solid lines. The dashed lines follow from the asymptotic ($R_1 \ll 1$) formula [2, eq. (4.185)].

Remark 3.7. As discussed in [3, p. 179], roots of (7) approximate eigenvalues λ of both Neumann's (1) and Dirichlet's

$$-\nabla^2\varphi = \lambda\varphi \ \text{ in } \ D; \ \ \varphi = 0 \ \text{ on } \ \partial D \tag{8}$$

spectral boundary problems. Readers can justify this fact (after a rather tedious derivation) for circular and annular tanks when analytical solutions exist. *A posteriori* numerical procedure is therefore needed to select which of computed λ correspond to (1).

Remark 3.8. The spectral problem (1) possesses degenerate eigenvalues (the second-order multiplicity) for circular, annular, and any other cross-section that is invariant relative to the $\pi/2$-rotation. For that case, the determinant of (7) does not change the sign at the corresponding λ that means a difficulty in a numerical detection of its zeros. One can then focus on finding the minima of the determinant modulus [1]. Alternatively, the weight coefficients in (2) may be recombined to provide, *a priori*, the required eigenfunction symmetry excluding, thereby, the multiplicity.

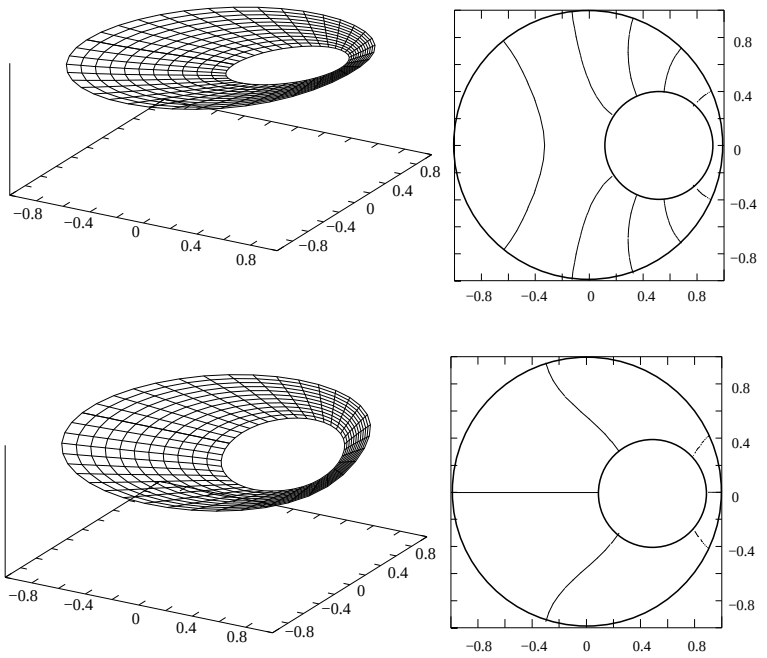

Fig. 3. Two eigenfunctions $\varphi(x,y;\lambda_{11}^{\cos})$, the first row, and $\varphi(x,y;\lambda_{11}^{\sin})$, the second row, for the case in fig. 2 with $R_1 = 0.4$. Three-dimensional and topographic views.

Remark 3.9. Computing integrands in (6) requires to know, explicitly, $\nabla\phi_{k,i}|_{\Gamma_l}$ and $\phi_{k,i}|_{\Gamma_l}$ as functions of θ_l for all $0 < k < M$ ($\boldsymbol{n}_0 = (\cos\theta_0, \sin\theta_0)$ and $\boldsymbol{n}_l = -(\cos\theta_l, \sin\theta_l)$). Originally, $\phi_{k,i}$ and $\nabla\phi_{k,i} = (\partial_x\phi_{k,i}, \partial_y\phi_{k,i})$,

$$\begin{aligned}\partial_x\phi_{k,i} &= \partial_{x_k}\phi_{k,i} = \cos\theta_k\,\partial_{r_k}\phi_{k,i} - r_k^{-1}\sin\theta_k\,\partial_{\theta_k}\phi_{k,i},\\ \partial_y\phi_{k,i} &= \partial_{y_k}\phi_{k,i} = \sin\theta_k\,\partial_{r_k}\phi_{k,i} + r_k^{-1}\cos\theta_k\,\partial_{\theta_k}\phi_{k,i},\end{aligned} \tag{9}$$

are functions of the polar coordinates (r_k, θ_k) where $r_k = \sqrt{x_k^2 + y_k^2}$, $\theta_k = \mathrm{atan2}(y_k, x_k)$ (atan2 is the acrtangent function of two arguments well–known in the computer languages) in terms of the local Cartesian coordinate system $O_k x_k y_k$. However, substituting $x_k = x_{0l} - x_{0k} + R_l\cos\theta_l$, $y_k = y_{0l} - y_{0k} + R_l\sin\theta_l$ makes them exclusively depending on $0 \le \theta_l < 2\pi$.

4. Numerical examples

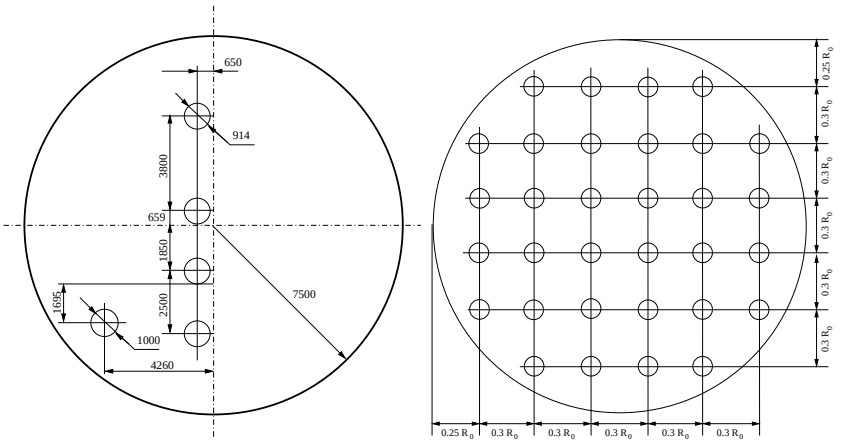

Fig. 4. *The left panel*: A simplified cross-sectional plane of the Draugen platform shaft (see, the actual geometry in fig. 1) considered in [2, sect. 4.11.5] suggesting that pipes of lower radii are neglected. Dimensions are in mm. *The right panel:* A sample cross-sectional domain considered in [1] includes a symmetric (with respect to the coordinate axes) array of equal poles of the radius R_i, $i = 1, \ldots, 32$.

A single eccentric pole with the 1/2–offset is considered with a focus on the two lowest eigenvalues $\lambda_{11}^{\sin}$ and $\lambda_{11}^{\cos}$ splitting from the two equal lowest eigenvalues $\lambda_{11} = 1.841\ldots$; $J_1'(\lambda_{11}) = 0$ which correspond to eigenfunctions $J_1(\lambda_{11} r)\sin\theta$ and $J_1(\lambda_{11} r)\cos\theta$. The numerical results are shown in fig. 2 by the solid lines *versus* the nondimensional pole radius, $0 < R_1 < 0.5$. These are consistent with computations in [1] (boundary element method); difference is invisible when superposing the graphs. In addition, the dashed lines are drawn determined by the asymptotic formula [2, eq. (4.185)] which is derived by combining the Rayleigh quotient formulation and the strip theory (the result depends on h, the deep water approximation is used). Fig. 2 shows that the lowest $\lambda_{11}^{\sin}$ monotonically decreases and using [2, eq. (4.185)] provides a good approximation of this eigenvalue for $R_1 \lesssim 0.2$. However, the second eigenvalue $\lambda_{11}^{\cos}$ is not accurately approximated by the asymptotic formula; the function $\lambda_{11}^{\cos}(R_1)$ is not monotonic but the formula does not fit that. The corresponding eigenfunctions are shown in fig. 3 by the three-dimensional

Table 1. The sample case in the right panel of fig. 4 suggesting 32 poles of the equal radii R_i, $i = 1, ..., 32$. The poles are located symmetrically with respect to the Cartesian axes so that the lowest eigenvalue implies two natural sloshing modes. The computed lowest eigenvalue λ_{11} by the Trefftz method (second column) is compared with the deep water prediction by the formula [2, eq. (4.185)] (third column) and the boundary element (BE) computations in [1] (columns 4-6) conducted with different numbers of facets per pipe (pole) while 60 facets per the outer circle is used. The framed numbers correspond to the exact solution detected by our method and the asymptotic formula [2, eq. (4.185)].

	present computations		BEM [1], 60 facets/ outer circle		
R_i/R_0	Trefftz app.	[2, eq. (4.185)]	6 fac./pipe	12 fac./pipe	24 fac./pipe
0.0000	1.8412...	1.8412...	1.847	1.847	1.847
0.0125	1.8359	1.8359	1.840	1.841	1.842
0.0250	1.8202	1.8201	1.818	1.823	1.825
0.0375	1.7946	1.7935	1.783	1.794	1.798
0.0500	1.7602	1.7542	1.736	1.755	1.761
0.0625	1.7178	1.7043	1.677	1.706	1.716
0.0750	1.6685	1.6253	1.607	1.649	1.663

and topographic views. The function $\varphi(x, y; \lambda_{11}^{\cos})$ is even by y and the associated liquid flows mainly occur "along" the Ox-axis. The proximity effect (between the tank walls and the pole) may matter causing the non-monotonic character of the $\lambda_{11}^{\cos}(R_1)$ as R_1 tends to 0.5. The lowest natural sloshing mode is odd by y, $\varphi(x, y; \lambda_{11}^{\sin}) = -\varphi(x, -y; \lambda_{11}^{\sin})$.

An example from [2, sect. 4.11.5] is considered which appears after excluding all pipes of lower diameters from the Draugen platform shaft. This simplification is shown in the left panel of fig. 4 (compare it with the actual cross–sectional plane in fig. 1). The highest natural sloshing period for the clean (without pipes) shaft is $T_1 = 4.04881$ s that corresponds to the two degenerating natural sloshing modes, $\varphi(x, y; \lambda_{11}) = J_1(\lambda_{11} r) \cos\theta$ and $J_1(\lambda_{11} r) \sin\theta$. This natural sloshing period T_1 splits, according to our computations, to $T_1^* = 4.10807$ s and $T_1^{**} = 4.06965$ s. The highest period T_1^* was approximated in [2, sect. 4.11.5] by the asymptotic formula [2, eq. (4.185)]. The asymptotic result is 4.111 s.

Computations were done for the perforated domain in the right panel of fig. 4. This sample geometry was introduced and analysed in [1]. Table 1 compares our computations with [1] and the asymptotic formula [2, eq. (4.185)]. Our numerical method (the asymptotic formula as well) fits

the exact solution for the clean tank ($R_i/R_0 = 0$, framed numbers) but [1] clearly overpredicts the corresponding exact eigenvalue, most probably, due to a slow convergence of the boundary element method. The formula [2, eq. (4.185)] remains rather accurate for the lower poles radii.

5. Conclusions

A semi-analytical approximation of the natural sloshing modes in an upright circular cylindrical tank equipped with vertical poles can be obtained by applying a variational Trefftz method to the corresponding spectral boundary problem formulated in the cross–sectional plane. The method employs the Bessel–type functional basis parametrically depending on the spectral parameter. The spectral parameter appears in a nonlinear manner and the solvability condition yields a transcendental equation with respect to the parameter. The equation turns to the well-known form when the exact analytical solution exists. Numerical examples demonstrate the accuracy and effectiveness of the proposed method. Comparisons are made with computations in [1] and the asymptotic formula [2, eq. (4.185)] approximating the lowest natural sloshing frequencies.

[1] *Drake K.* The effect of internal pipes on the fundamental frequency of liquid sloshing in a circular tank // Applied Ocean Research.— 1999.— **21**.— P. 133–143.

[2] *Faltinsen O. M., Timokha A. N.* Sloshing.— Cambridge University Press, 2009.— 686 p.

[3] *Faltinsen O. M., Timokha A. N.* Analytically approximate natural sloshing modes and frequencies in two-dimensional tanks // European Journal of Mechanics. B/Fluids.— 2014.— **47**.— P. 176–187.

[4] *Ibrahim R.* Liquid sloshing dynamics.— Cambridge University Press, 2005.— 900 p.

[5] *Li T. F., Lin C. C., Luk C.* Three-directional fluid pool seismic sloshing analysis // ASME Journal of Pressure Vessel Technology.— 1981.— **103**.— P. 10–15.

[6] *Lukovsky I. A.* Nonlinear Dynamics: Mathematical Models for Rigid Bodies with a Liquid.— De Gruyter, 2015.— 400 p.

[7] *Takahara H., Hara K., Ishida T.* Nonlinear liquid oscillation in a cylindrical tank with an eccentric core barrel // Journal of Fluids and Structures.— 2012.— **35**.— P. 120–132.